Supplementary Information (SI) for ChemComm.

Supplementary Information

Can reconfiguring the band-edge states regulate excitonic states in two-dimensional superlattice perovskites?

Heng Cao[1], Qingjie Feng[1], Guangjun Nan[1,*]

[1] Department of Physics, Zhejiang Normal University, Jinhua, Zhejiang 321004, P. R. China

*Corresponding authors: E-mail: gjnan@zjnu.edu.cn

This file includes

Texts S1 to S2

Tables S1 to S2

Figs S1 to S13

Text S1. Computational details

The ground-state geometry optimization of 2D superlattice perovskites is performed by using the density functional theory (DFT) approach, which can be implemented with the Vienna Ab initio Simulation Package.[1,2] The electronic exchange–correlation potential is treated by the Perdew–Burke–Ernzerhof generalized gradient approximation.[3] The core electrons are described by using the projector augmented-wave method[4] while the valence electron wave functions are projected onto plane-wave basis sets with a kinetic energy cutoff value of 400 eV. The 4 × 4 × 1 Monkhorst−Pack *k*-point mesh is adopted to sample the first Brillouin zone. The convergence threshold for the residual forces on ions and the energy differences between successive electronic self-consistent field cycles are set as 0.01 eV $Å^{-1}$ and 10^{-5} eV, respectively. In these calculations, the van der Waals corrections are taken into account by using the semi-empirical DFT-D2 method,[5] which is demonstrated to be reliable for calculating the lattice parameters and electronic structures in 2D perovskites.[6] The DFT-relaxed lattice parameters are demonstrated to well match those by the Equation of State (EOS) analysis (Fig. S1). The convergences of the kinetic energy cutoff value and *k*-point sampling are also confirmed, which are shown in Figs. S2-S4. Based on the relaxed ground-state geometries, the high-frequency dielectric constant is calculated according to the approach of Gajdoš et al.[7] Projected density of states (PDOS) and frontier orbitals are computed by combining a modified version of the HSE06 functional[8] which includes 43% Hartree-Fock exchange[9] and spin-orbit coupling (SOC) corrections. Subsequently, photogenerated electron-hole distributions in the lowest-energy excitonic state of the studied 2D superlattice perovskites are achieved by adopting the timed-dependent DFT (TDDFT) method with an optimally-tuned,[10,11] screened and range-separated hybrid (OTSRSH) functional.[12-15] Formulated with spinor wavefunctions,[16] the TDDFT-OTSRSH method can not only capture the long-range electron-electron and electron-hole interactions, but treat the SOC corrections in solids. The formalism of the TDDFT methods with the OTSRSH functional is shown in the text S2.

Text S2. Formalism of time-dependent density functional theory method

Formulated with spinor wavefunctions,[16] the following non-Hermitian eigenvalue equation is solved to determine the exciton energies and wavefunctions:[17]

$$\begin{pmatrix} \boldsymbol{A} & \boldsymbol{B} \\ \boldsymbol{B}^{*} & \boldsymbol{A}^{*} \end{pmatrix} \begin{pmatrix} \boldsymbol{X_I} \\ \boldsymbol{Y_I} \end{pmatrix} = \omega_I \begin{pmatrix} \boldsymbol{1} & 0 \\ 0 & -\boldsymbol{1} \end{pmatrix} \begin{pmatrix} \boldsymbol{X_I} \\ \boldsymbol{Y_I} \end{pmatrix} \tag{S1}$$

where the pseudo-eigenvalue ω_I denotes the I-th exciton energy. According to the basis of two-component spinor orbitals ($ij\sigma$), the matrix elements of $\boldsymbol{A}$ and $\boldsymbol{B}$ are given as:

$$A_{ij\sigma,kl\tau} = \delta_{i,k}\delta_{j,l}(\varepsilon_j - \varepsilon_i) + K_{ij,kl} \tag{S2}$$

$$B_{ij,kl} = K_{ij,lk}. \tag{S3}$$

Here, K is the coupling matrix where indices i and k indicate the occupied Kohn-Sham (KS) orbitals, and j and l represent the virtual KS orbitals. Based on the assignment ansatz of Casida, the many-body wavefunction of an excited state I is expressed as

$$\Phi_I \approx \sum_{ij\sigma} \frac{X_{I,ij\sigma}+Y_{I,ij\sigma}}{\sqrt{\omega_I}} \hat{a}_{j\sigma}^{\dagger}\hat{a}_{i\sigma}\Phi_0 = \sum_{ij\sigma} Z_{I,ij}\, \hat{a}_{j\sigma}^{\dagger}\hat{a}_{i\sigma}\Phi_0, \tag{S4}$$

where $Z_{I,ij} = (X_{I,ij} + Y_{I,ij})/\sqrt{\omega_I}$, $\hat{a}_{i\sigma}$ is the annihilation operator acting on the i-th KS orbital with spin σ, and Φ_0 is the ground-state many-body wavefunction taken to be the single-Slater determinant of the occupied KS orbitals. Based on the many-body wavefunctions, the charge density associated with the exciton states is written as[18]

$$\rho_I = \sum_{ijj'} Z_{I,ij}^{*} Z_{I,ij'}\, \phi_j^{*}\phi_{j'} - \sum_{ii'j} Z_{I,ij}^{*} Z_{I,i'j}\, \phi_{i'}^{*}\phi_i, \tag{S5}$$

where ϕ_i is KS orbital.

To assess a reasonable energy level alignment of frontier orbitals contributed by organic spacer layer and inorganic layer in the 2D superlattice perovskites, the OTSRSH functional is resorted in this work. Specifically, the Coulomb repulsion operator $1/r$ is divided into a short-range and a long-range part by using the error function

$$\frac{1}{r}=\frac{\alpha+\beta\,\mathrm{erf}(\mu r)}{r}+\frac{1-\alpha-\beta\,\mathrm{erf}(\mu r)}{r} \tag{S6}$$

where r represents the distance between electrons, erf(μr) is the Gaussian error function with μ being a range-separation parameter. The α and β are tunable parameters with α determining the contribution from the exact exchange and β controlling the contribution from the long-range exchange terms. α and β satisfy the requirement of $\alpha + \beta = 1/\varepsilon_0$ where ε_0 is the scalar dielectric constant of the solid. The anisotropy of the dielectric constant is neglected, which is anticipated to little impact our conclusions.[19] The Fock-like exchange and semi-local KS exchange functional are applied to treat the first and second term at the right-hand side, respectively. Then, the OTSRSH exchange correlation potential is given by[15]

$$V_{\mathrm{xc}}^{\mathrm{RSH}}=\alpha V_{\mathrm{Fx}}+\beta V_{\mathrm{Fx}}^{\mathrm{LR}}+(1-\alpha)V_{\mathrm{KSx}}-\beta V_{\mathrm{KSx}}^{\mathrm{LR}}+V_{\mathrm{KSc}}. \tag{S7}$$

Here, LR represents the long-range terms, Fx labels Fock-like exchange, KSx and KSc labels semi-local KS exchange and correlation, respectively. In order to reduce the computational cost associated with the Fock-like exchange on large systems, the first-order perturbation theory to the range-separated hybrid KS Hamiltonian is employed.[20] According to the high-frequency dielectric constant calculated in this work (Fig. S10), the set of the parameters (α = 0.07, ε_0 = 5 and μ = 0.03) is used for the studied $(FBTT)_2Pb_2Br_6$ perovskites. This is due to that the energy level alignment of $(FBTT)_2Pb_2Br_6$ is reasonably predicted by the DFT-OTSRSH method when compared with the experiments[21] and is highly consistent with that calculated at the DFT-HSE06 level of theory when the SOC effect is excluded (Fig. S9). Considering that the high-frequency dielectric constants change slightly in the studied systems, these parameters are fixed for the studied materials in this work.

Table S1. DFT-optimized lattice parameters for the unit cells of the studied $A_2Pb_2X_6$ (A = FBTT, FPT, FNT; X = Cl, Br, I) 2D superlattice perovskites. The values in parenthesis denote the lattice parameters which are fitted according to the third-order Brich-Murnaghan EOS analysis in Fig. S1.[22,23]

$A_2Pb_2X_6$ (A = FBTT, FPT, FNT; X = Cl, Br, I)	Bond length (Å)			Bond angle (°)		
	a	b	c	α	β	γ
$(FBTT)_2Pb_2Cl_6$	7.81	10.42	30.91	91.75	90.22	91.86
$(FPT)_2Pb_2Cl_6$	7.81	10.42	30.91	91.75	90.22	91.86
$(FNT)_2Pb_2Cl_6$	7.81	10.42	30.91	91.75	90.22	91.86
$(FBTT)_2Pb_2Br_6$	7.91	10.52	30.94	91.87	90.47	91.99
	(8.05)	(10.82)	(31.56)	(91.82)	(90.95)	(91.76)
$(FPT)_2Pb_2Br_6$	7.91	10.52	30.94	91.87	90.47	91.99
$(FNT)_2Pb_2Br_6$	7.91	10.52	30.94	91.87	90.47	91.99
$(FBTT)_2Pb_2I_6$	8.05	10.76	30.96	92.03	90.54	91.89
$(FPT)_2Pb_2I_6$	8.05	10.76	30.96	92.03	90.54	91.89
$(FNT)_2Pb_2I_6$	8.05	10.76	30.96	92.03	90.54	91.89

Table S2. Exciton binding energies (namely the energy differences between fundamental gap and optical gap) of four superlattice perovskites with different energy level alignments.

$A_2Pb_2X_6$ (A = FBTT, FPT; X = Cl, Br, I)	Exciton binding energies (eV)
$(FPT)_2Pb_2Cl_6$	0.48
$(FBTT)_2Pb_2Br_6$	0.40
$(FBTT)_2Pb_2I_6$	0.47
$(FPT)_2Pb_2I_6$	0.41

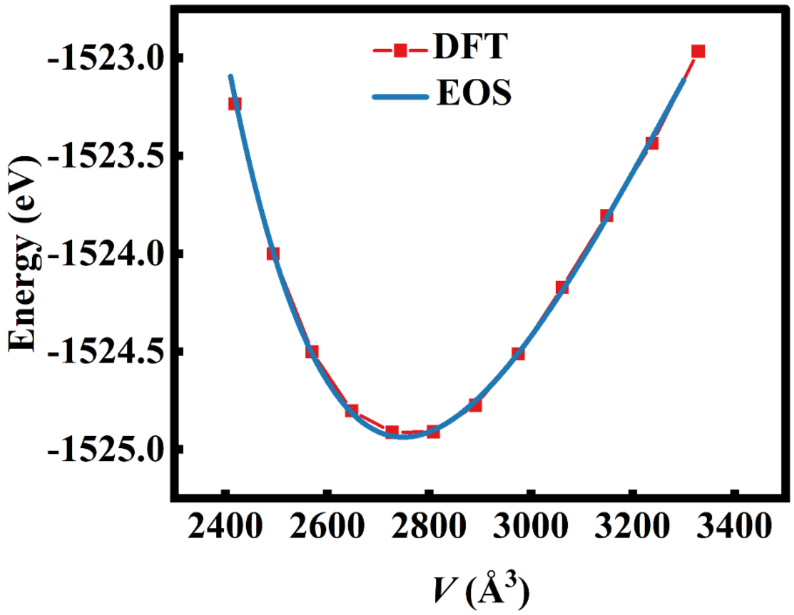

Fig. S1 Energy (E) versus volume (V) curve of $(FBTT)_2Pb_2Br_6$ structure by performing third-order Brich-Murnaghan EOS analysis with the expression $E(V) = E_0 + \frac{9V_0B_0}{16}\left\{\left[\left(\frac{V_0}{V}\right)^{\frac{2}{3}} - 1\right]^3 B_0' + \left[\left(\frac{V_0}{V}\right)^{\frac{2}{3}} - 1\right]^2 \left[6 - 4\left(\frac{V_0}{V}\right)^{\frac{2}{3}}\right]\right\}$. Here, E_0 and V_0 are the energy and volume at equilibrium, B_0 is the bulk elastic modulus and B_0' is the first derivative of the bulk elastic modulus to volume.

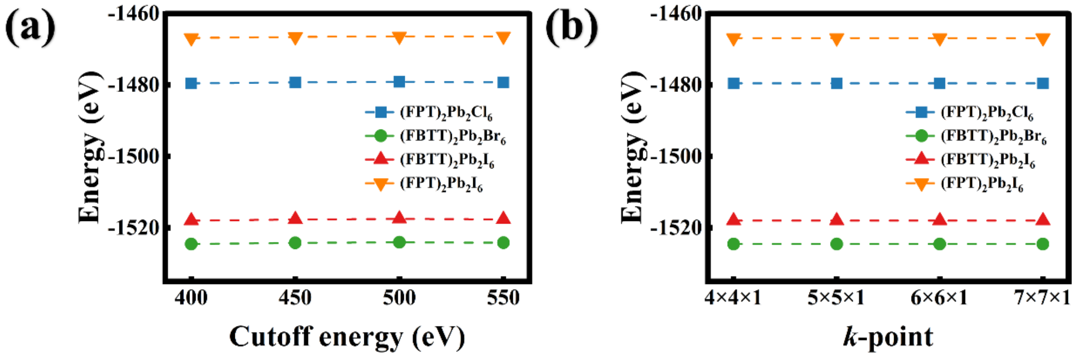

Fig. S2 Convergence tests for total energies by changing kinetic energy cutoffs and *k*-point meshes. (a) Total energies calculated by using four cutoff energies with the 4 × 4 × 1 *k*-point mesh. (b) Total energies calculated by sampling the first Brillouin zone with four *k*-point meshes when the cutoff energy is set to be 400 eV.

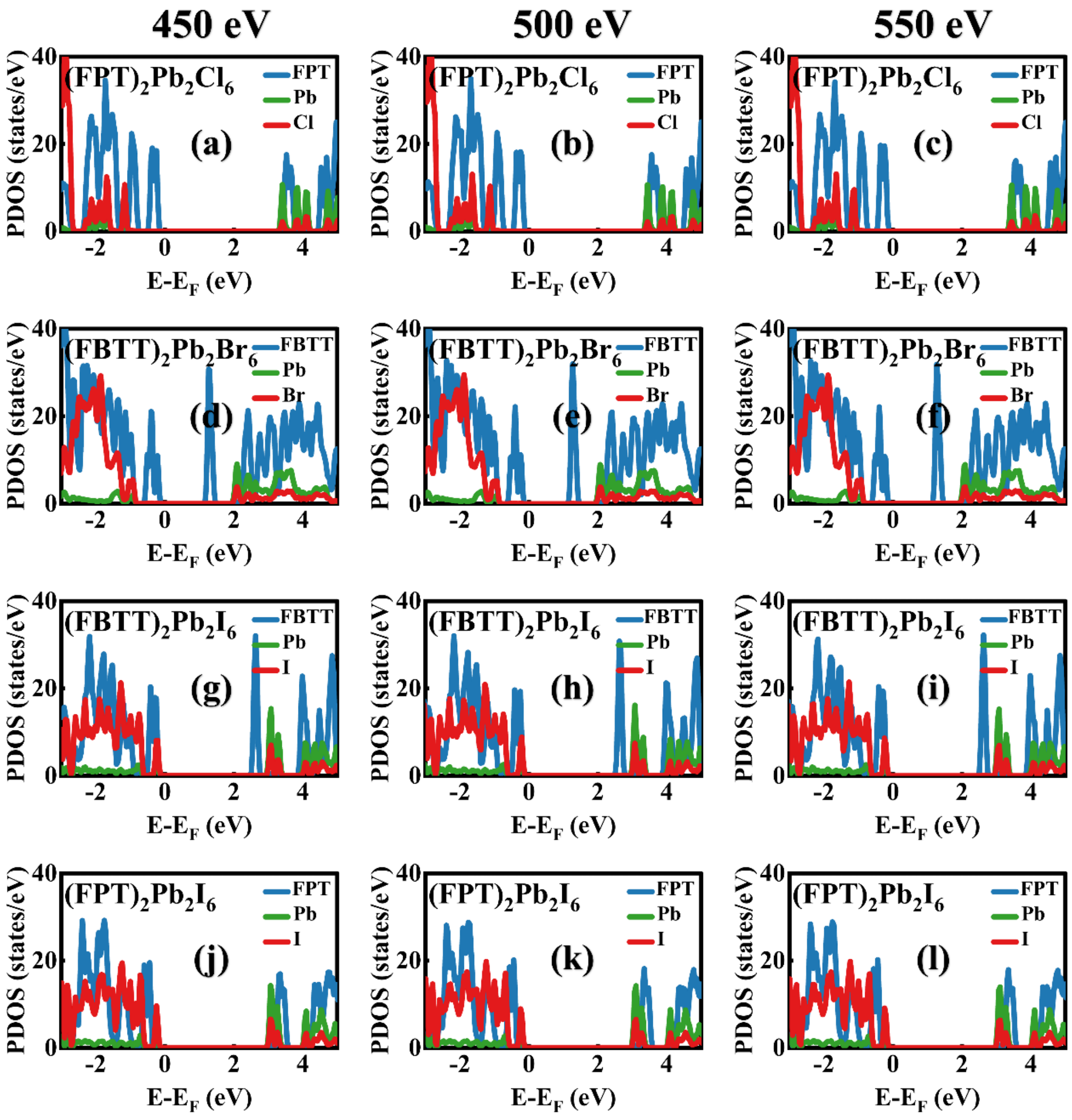

Fig. S3 The PDOS of the (FPT)$_2$Pb$_2$Cl$_6$, (FBTT)$_2$Pb$_2$Br$_6$, (FBTT)$_2$Pb$_2$I$_6$ and (FPT)$_2$Pb$_2$I$_6$ systems which shown different energy level alignments. These are calculated at the HSE06+SOC level of theory with cutoff energies of 450, 500, and 550 eV when the 4 × 4 × 1 mesh is used, suggesting that the change of cutoff energies does not influence the energy level alignments shown in Fig. 2.

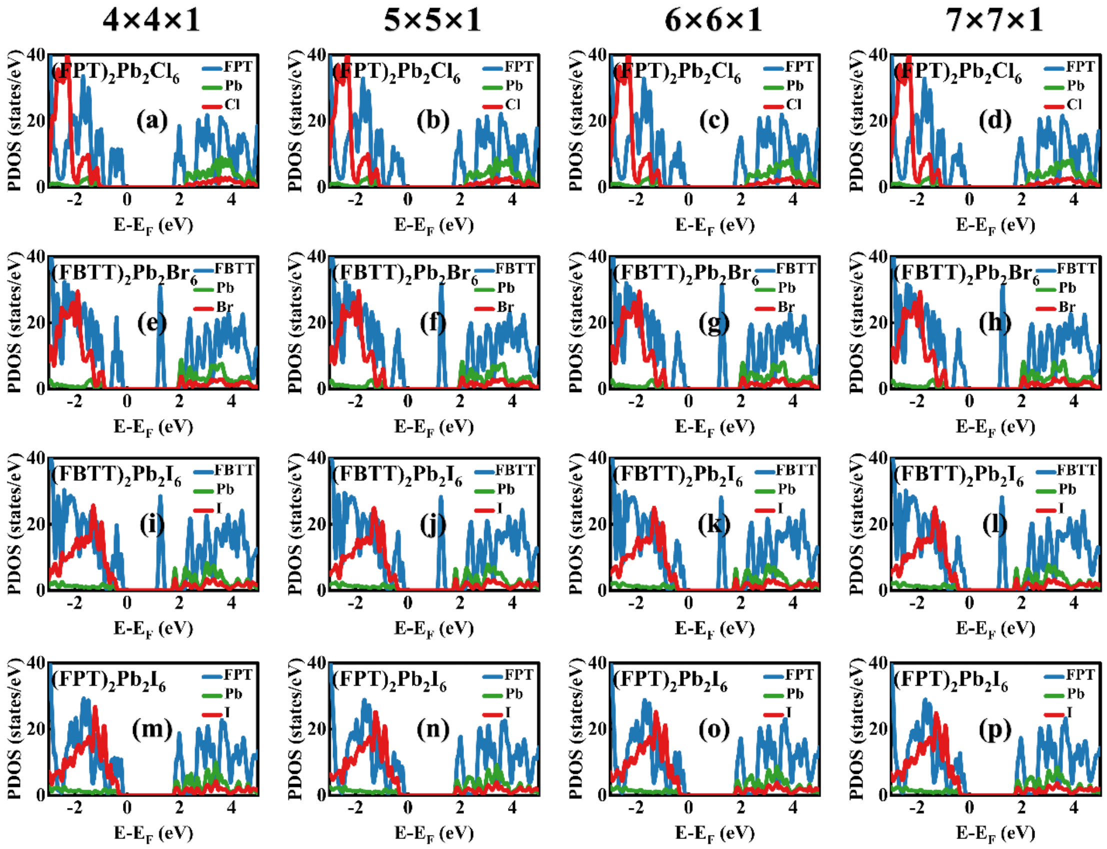

Fig. S4 The PDOS for the (FPT)$_2$Pb$_2$Cl$_6$, (FBTT)$_2$Pb$_2$Br$_6$, (FBTT)$_2$Pb$_2$I$_6$ and (FPT)$_2$Pb$_2$I$_6$ superlattice perovskites. Given the expensive cost of HSE06+SOC level of theory, the PBE functional is employed to test the convergence of *k*-point densities which include 4 × 4 × 1, 5 × 5 × 1, 6 × 6 × 1, and 7 × 7 × 1 meshes when the cutoff energy is set to be 400 eV.

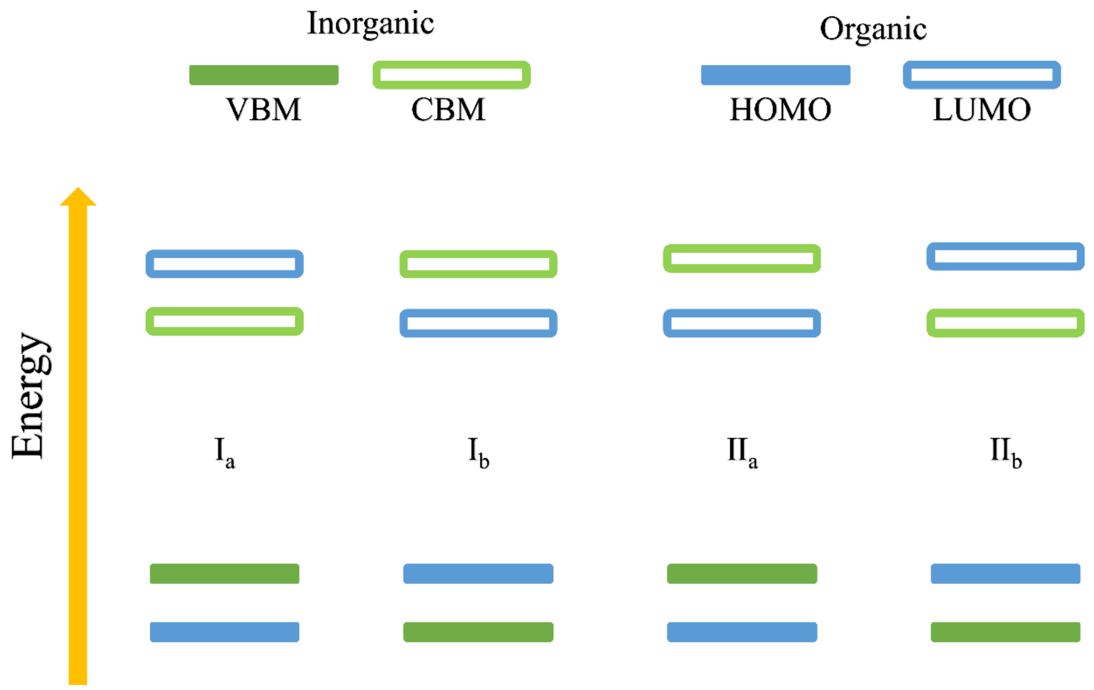

Fig. S5 Schematic diagram of different types of energy level alignments in 2D perovskites.

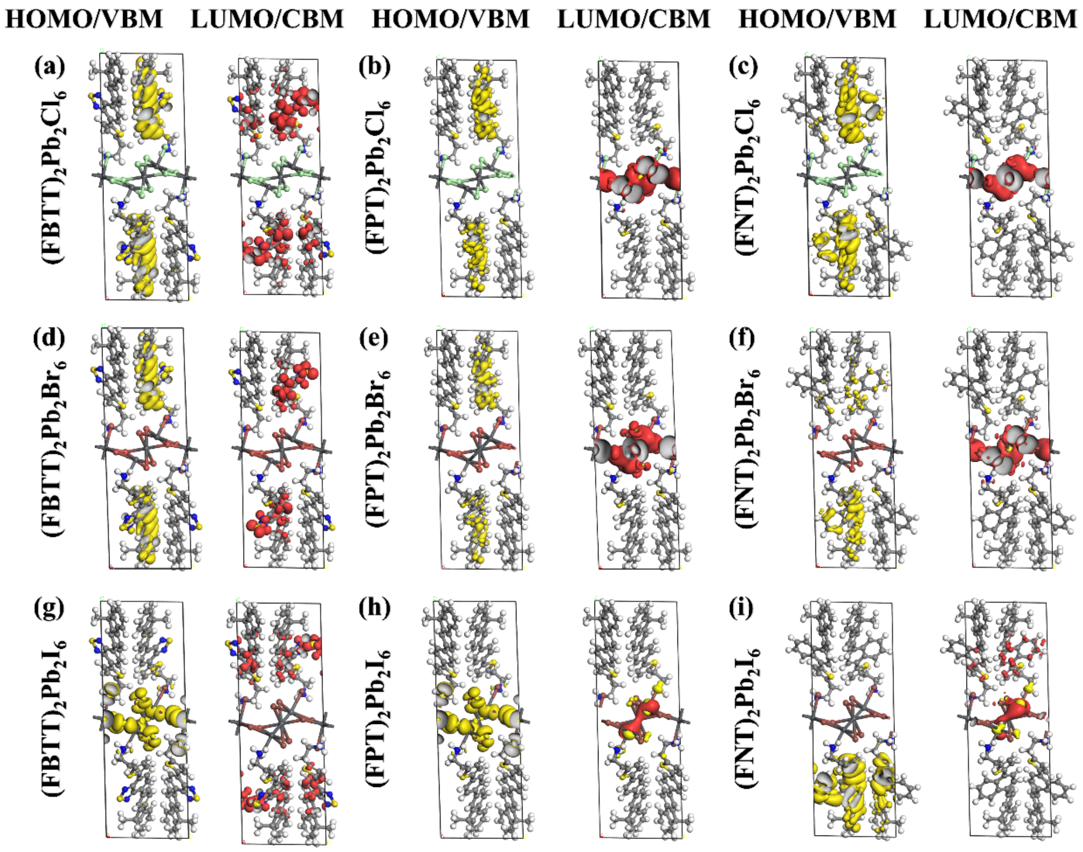

Fig. S6 Frontier orbitals of the studied 2D superlattice perovskites in pristine structures.

The iso-surface value of the frontier orbitals is 3.0 ×10^{-3} e Å^{-3}.

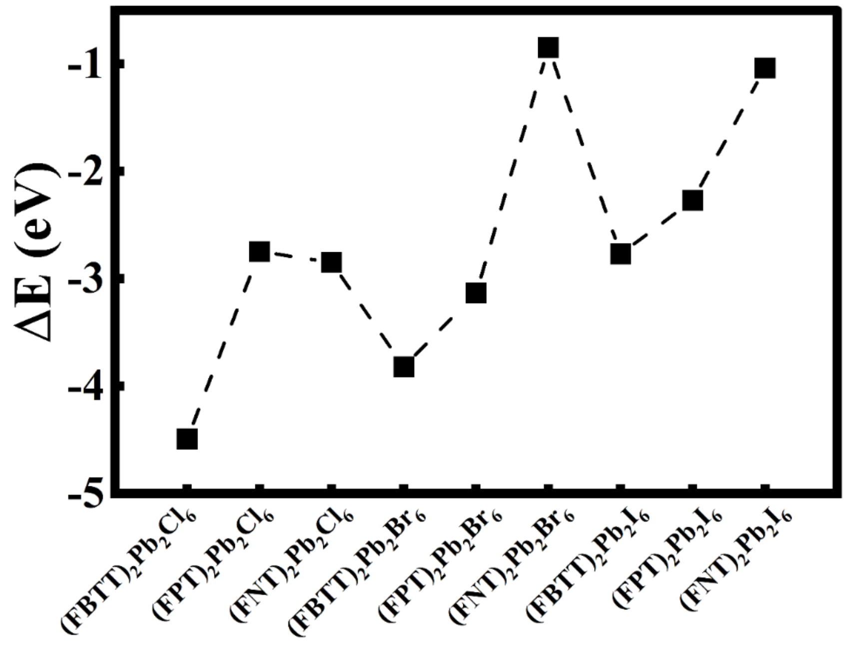

Fig. S7 Energy differences (ΔE = $E_{pristine}$ - $E_{stretched}$) of ground-state energies between pristine and stretched structures of the studied 2D superlattice perovskites.

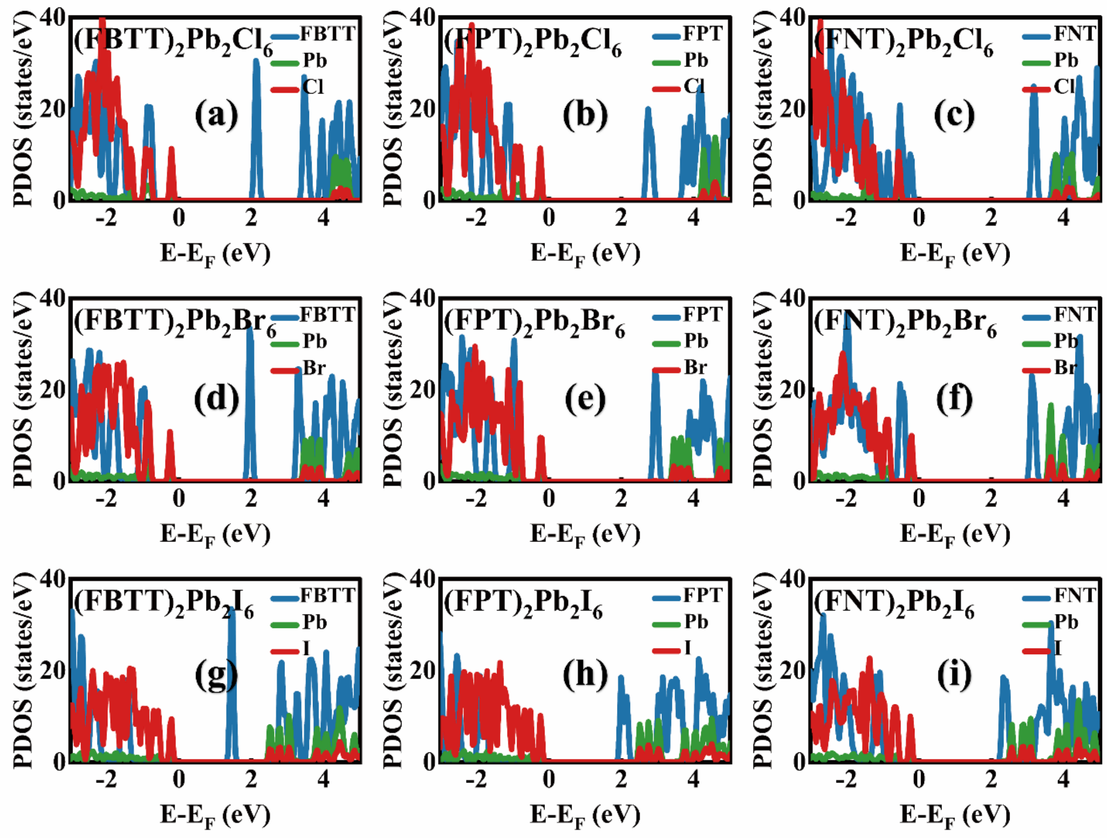

Fig. S8 PDOS calculated at the HSE06+SOC level of theory for the studied 2D superlattice perovskites with stretched structures.

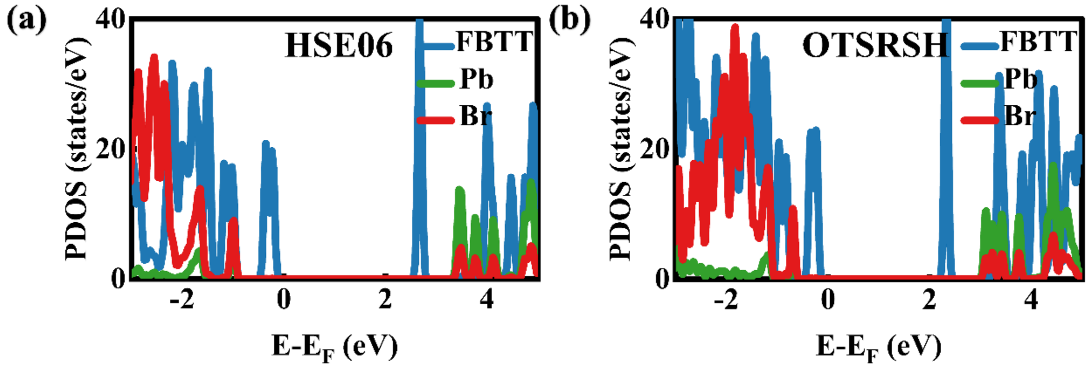

Fig. S9 PDOS calculated with (a) HSE06 and (b) OTSRSH functionals for $(FBTT)_2Pb_2Br_6$ perovskite.

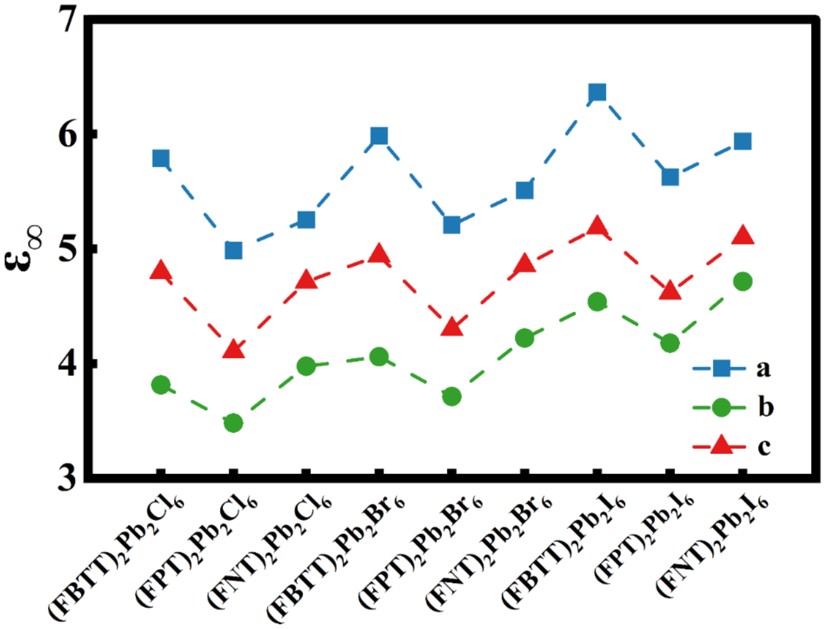

Fig. S10 The calculated high-frequency dielectric constants (ε_∞) along a, b and c axis for the studied 2D superlattice perovskites.

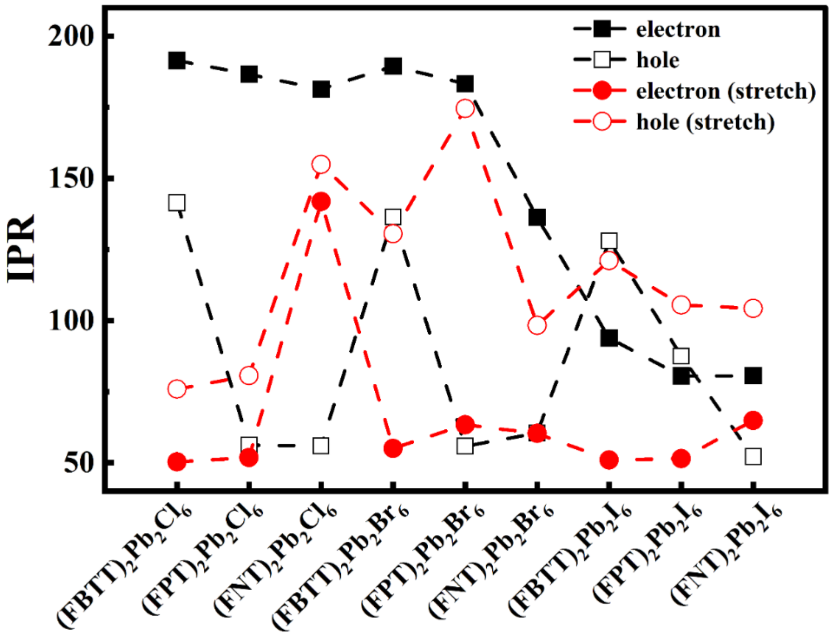

Fig. S11 IPRs of the electron and hole densities according to the frontier orbitals shown in Figs. S6 and S13.

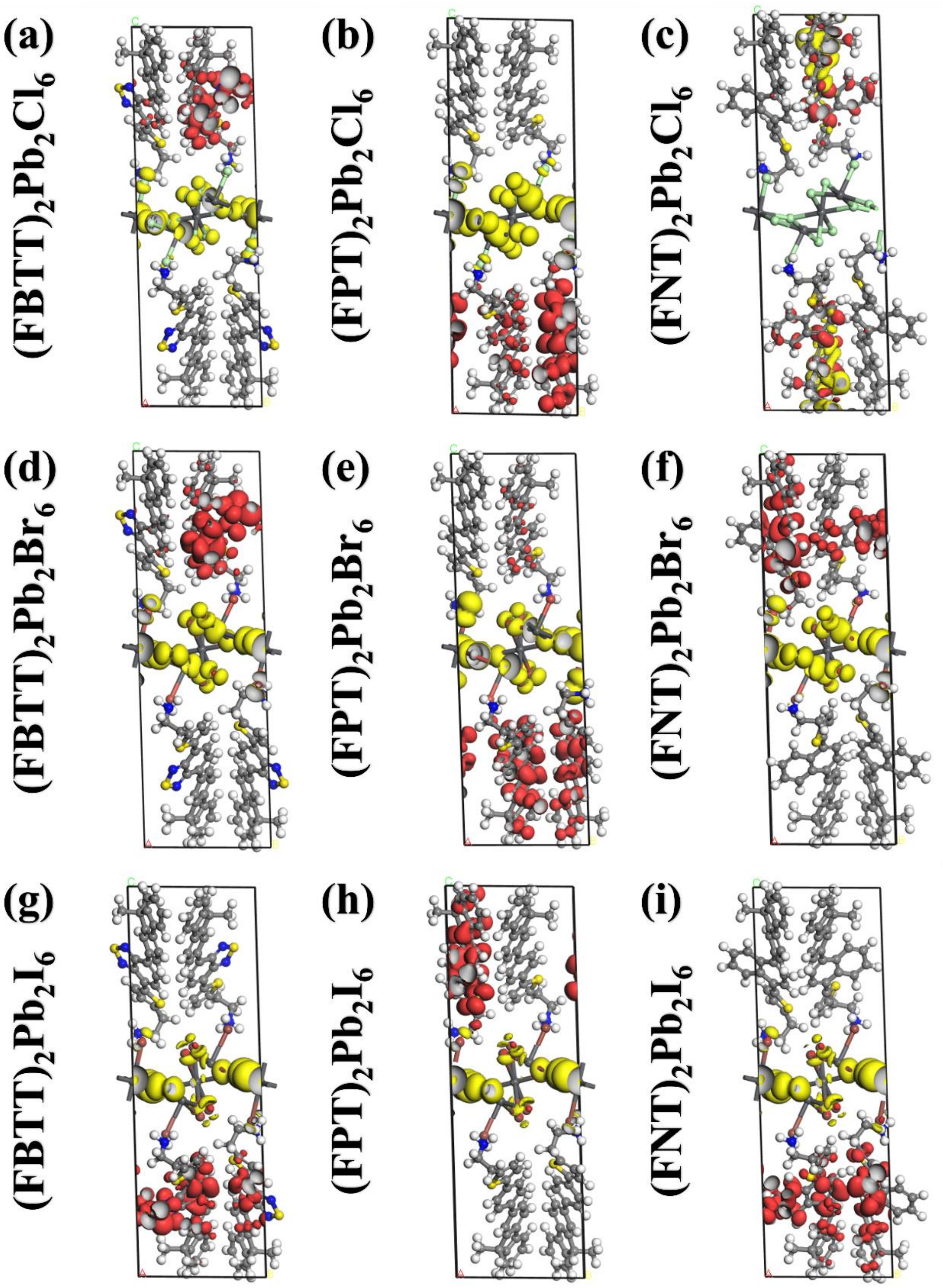

Fig. S12 Photoexcited e-h densities in the lowest-energy excitonic state of the studied 2D superlattice perovskites with stretched structures. The electron (hole) densities are shown in red (yellow) with the iso-surface value being 3.0×10^{-3} e Å^{-3}.

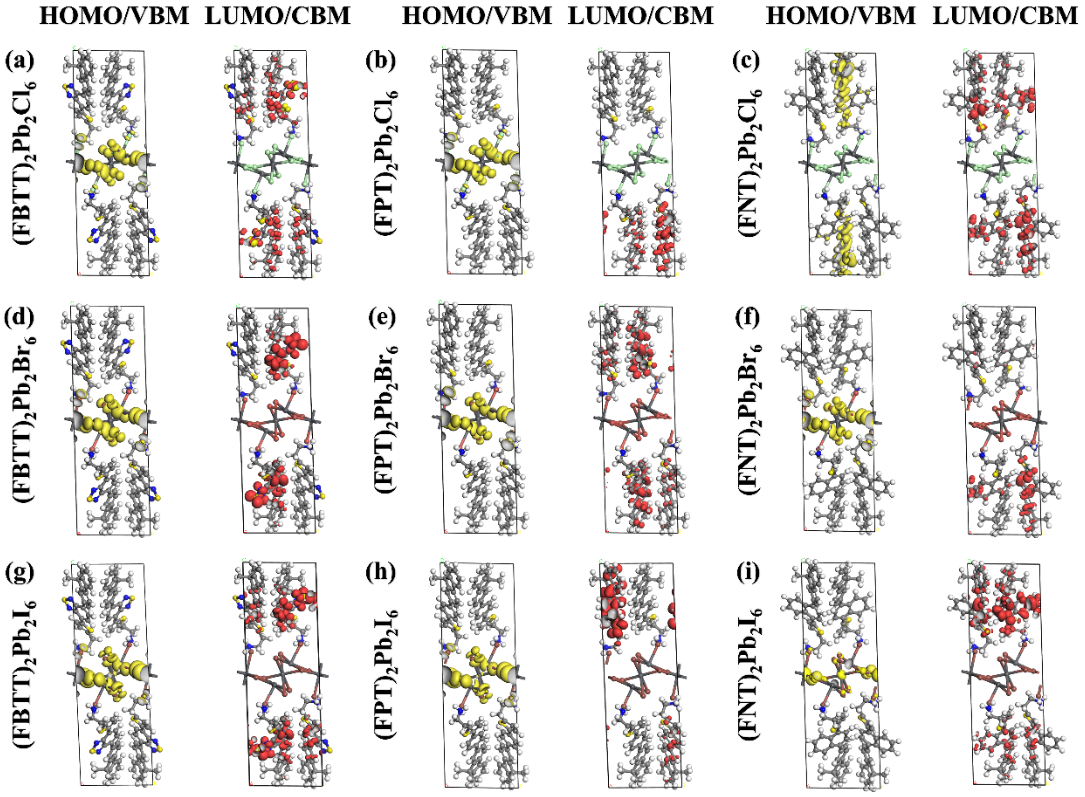

Fig. S13 Frontier orbitals of the studied 2D superlattice perovskites with stretched structures. The iso-surface value of the frontier orbitals is 3.0 $\times 10^{-3}$ e Å^{-3}.

Reference

1. G. Kresse and J. Furthmüller, *Comput. Mater. Sci.*, 1996, **6**, 15-50.
2. G. Kresse and J. Hafner, *Phys. Rev. B*, 1993, **47**, 558-561.
3. J. P, Perdew, K. Burke and M. Ernzerhof, *Phys. Rev. Lett.*, 1996, **77**, 3865.
4. P. E. Blöchl, *Phys. Rev. B*, 1994, **50**, 17953-17979.
5. S. Grimme, *J. Comput. Chem.*, 2006, **27**, 1787-1799.
6. Q. Feng, X. Zhang and G. Nan, *Mater. Horiz.*, resubmitted.
7. M. Gajdoš, K. Hummer, G. Kresse, J. Furthmüller and F. Bechstedt, *Phys. Rev. B*, 2006, **73**, 045112.
8. J. Heyd, G. E. Scuseria and M. Ernzerhof, *J. Chem. Phys.*, 2003, **118**, 8207-8215.
9. C. Coccia, M. Morana, A. Mahata, W. Kaiser, M. Moroni, B. Albini, P. Galinetto, G. Folpini, C. Milanese, A. Porta, E. Mosconi, A. Petrozza, F. De Angelis and L. Malavasi, *Angew. Chem. Int. Ed.*, 2024, **63**, e202318557
10. E. K. U. Gross and W. Kohn, *Phys. Rev. Lett.*, 1985, **55**, 2850-2852.
11. M. Marques, N. Maitra, F. Nogueira, E. K. U. Gross and A. Rubio, *Fundamentals of Time-Dependent Density Functional Theory*, Springer Science & Business Media, Berlin, 2012.
12. S. Refaely-Abramson, S. Sharifzadeh, N. Govind, J. Autschbach, J. B. Neaton, R. Baer and L. Kronik, *Phys. Rev. Lett.*, 2012, **109**, 226405
13. D. Wing, J. B. Haber, R. Noff, B. Barker, D. A. Egger, A. Ramasubramaniam, S. G. Louie, J. B. Neaton and L. Kronik, *Phys. Rev. Mater.*, 2019, **3**, 064603.
14. S. Refaely-Abramson, S. Sharifzadeh, M. Jain, R. Baer, J. B. Neaton and L. Kronik, *Phys. Rev. B*, 2013, **88**, 081204(R).
15. S. Refaely-Abramson, M. Jain, S. Sharifzadeh, J. B. Neaton and L. Kronik, *Phys. Rev. B*, 2015, **92**, 081204(R).
16. J. Liu, G. Lu and X. Zhang, *J. Chem. Phys.*, 2023, **158**, 044116.
17. D. P. Chong, *Recent Advances in Density Functional Methods*, World Scientific, Singapore, 1995.
18. X. Zhang, Z. Li and G. Lu, *Phys. Rev. B*, 2011, **84**, 235208.
19. Y. Gao, M. Zhang, X. Zhang and G. Lu, *J. Phys. Chem. Lett.*, 2019, **10**, 3820-3827.
20. X. Zhang, Z. Li and G. Lu, *J. Phys.: Condens. Matter*, 2012, **24**, 205801.
21. K. Wang, Z.-Y. Lin, A. De, C. A. Kocoj, W. Shao, H. Yang, Z. He, A. H. Coffey, C. B. Fruhling, Y. Tang, D. Varadharajan, C. Zhu, Y. S. Zhao, A. Boltasseva, V. M. Shalaev, P. Guo, B. M. Savoie and L. Dou, *Nature*, 2024, **633**, 567-574.
22. F. Birch, *Phys. Rev.*, 1947, **71**, 809-824.
23. F. D. Murnaghan, *Proc. Natl. Acad. Sci.*, 1994, **30**, 244.